

Article

# Improved Capacitor Voltage Feedforward for Three-Phase LCL-Type Grid-Connected Converter to Suppress Start-Up Inrush Current

Shiying Zhou <sup>1</sup>, Xudong Zou <sup>1,\*</sup>, Donghai Zhu <sup>1</sup>, Li Tong <sup>2</sup> and Yong Kang <sup>1</sup>

<sup>1</sup> State Key Laboratory of Advanced Electromagnetic Engineering and Technology, School of Electrical and Electronic Engineering, Huazhong University of Science and Technology, Wuhan 430074, China; syqn81192@hust.edu.cn (S.Z.); zhudh@hust.edu.cn (D.Z.); ykang@mail.hust.edu.cn (Y.K.)

<sup>2</sup> Zhejiang Electric Power Corporation Research Institute, Hangzhou 310014, China; tonyhust@126.com

\* Correspondence: xdzou@mail.hust.edu.cn; Tel.: +86-27-8754-3071

Academic Editor: Gabriele Grandi

Received: 5 April 2017; Accepted: 12 May 2017; Published: 18 May 2017

**Abstract:** Three-phase active damping LCL-type grid-connected converters are usually used in distributed power generation systems. However, serious inrush current will be aroused when the grid-connected converter starts, especially in rectifier mode, if no effective control method is taken. The point of common coupling (PCC) voltage feedforward is usually used to suppress start-up inrush current. Unfortunately, it will introduce a positive feedback loop related to the grid current and grid impedance under weak grid conditions, and therefore, the grid current will be distorted and the system stability margin will be significantly reduced. To solve the above problems, this paper proposes a simple method based on a  $d$ -axis fundamental positive-sequence component of filter capacitor voltage feedforward, without extra sensors and software resources. With the proposed method, it is possible to suppress the start-up inrush current and maintain the grid current quality and system stability under weak grid conditions. The mechanism of start-up inrush current and the effectiveness of the method for inrush current suppression are analyzed in detail. Then, the influences of different feedforward methods on system stability are analyzed under weak grid conditions by the impedance model of grid-connected converter. Finally, experimental results verify the validity of the proposed method.

**Keywords:** capacitor voltage feedforward; LCL-type grid-connected converter; stability; start-up inrush current; weak grid

## 1. Introduction

With the increasing penetration of renewable energy into the grid, power quality and stability issues become more and more important. In distributed power generation system (DPGS), a grid-connected converter is usually used as the interface between the renewable energy and grid, which plays an important role in injecting high quality power into the grid [1–3]. For the grid-connected converter, an LCL filter is usually preferred to attenuate the switching frequency harmonics due to its having a higher harmonic attenuating ability than an L filter [4,5]. For the three-phase LCL-type grid-connected converter, the most widely used current control method is the proportional-integral (PI) control in  $dq$  frame [1,6].

Many areas for improving the control performance of the LCL-type grid-connected converter have been discussed. To suppress the resonance peak of the LCL filter and avoid the attendant power loss of passive damping, some active damping control algorithms have been discussed [7,8]. Among various active damping solutions, capacitor current feedback active damping is widely used for its

ease of implementation [4,9]. The suppression of the grid current harmonics caused by distorted grid voltage is discussed in [10–12], and control delay compensation is discussed in [13,14]. However, there is very little literature on its start-up performance, which is an indispensable part of grid-connected converter current control.

When the DPGS starts, for example, the direct-drive wind power generation system (DDWPGS), as shown in Figure 1, before the grid-connected converter begins to work, the DC-bus capacitor will be pre-charged through the antiparallel diodes of the switches, until the DC-bus voltage is slightly below the peak value of grid line voltage, but far below the DC-bus voltage reference. Then, the grid-connected converter starts in rectifier mode and continues to pre-charge the DC-bus capacitor, until the DC-bus voltage reaches its reference. Then, the generator side converter starts, with grid-connected converter running in the inverter mode. However, when running in rectifier mode, the grid-connected converter would cause serious inrush current at the start time if no effective control method is employed [15]. Such inrush current may result in triggering overcurrent protection, and even damage the switching devices.

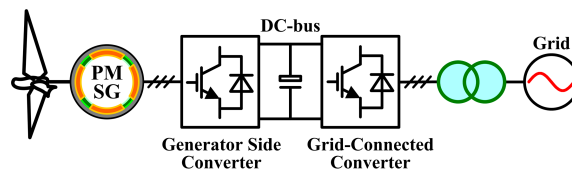


Figure 1. Direct-drive wind power generation system.

To suppress the start-up inrush current, for a grid-connected converter or pulse width modulation (PWM) rectifier, some control strategies have been studied. Reference [16] introduces constant terms into the current control loops to smooth the start-up behavior. Reference [17] proposes a method to pre-charge the DC-bus voltage until it reaches a certain level, at which point the conventional control strategy is adopted. However, these pre-charge methods are complicated. In [18], the current of the DC-bus capacitor is used as the reactive current reference during start-up. However, the inrush current is not particularly dependent on current reference when the converter starts, so such methods of current reference change cannot fundamentally suppress inrush current [15]. Reference [19] injects a reverse DC component current into the main circuit to mitigate the start-up inrush current. However, according to the simulation results in [19], this method can only accelerate attenuation of the inrush current, but cannot fundamentally suppress the generation of inrush current. As a consequence, grid voltage feedforward or filter capacitor voltage feedforward is usually used to fundamentally suppress start-up inrush current [6,15]. These methods are simple and easy to implement. However, since the renewable energy resources are usually located far from the load center, the public grid exhibits weak grid characteristics, which results in a situation where grid impedance cannot be ignored. Unfortunately, the applicability of the above methods under weak grid conditions has not been studied in the above references.

When the grid-connected converter is connected to a weak grid, the power quality and system stability will be significantly affected [3,4]. Generally, the short circuit ratio (SCR) is used to characterize the stiffness of the grid. When  $2 \leq \text{SCR} \leq 3$ , the grid is weak, and when  $\text{SCR} < 2$ , the grid is very weak [20]. Impedance-based control strategies and stability analysis under weak grid conditions are discussed in [4,21]. The negative effect of phase-locked loop (PLL) on the grid-connected converter control under weak grid conditions is discussed in [20,21]. Moreover, in [5], the influence of point of common coupling (PCC) voltage feedforward on the grid current control under weak grid conditions is studied. It concludes that PCC voltage feedforward will introduce a positive feedback loop related to the grid current and grid impedance, thus many grid current harmonics will be aroused and the system stability margin will be significantly reduced under weak grid conditions. In [22], it is pointed out that grid current control and the PCC voltage feedforward interact with each other via grid impedance.

Therefore, it is necessary to further study how to suppress start-up inrush current without impairing grid current quality and system stability under weak grid conditions.

For these issues, this paper proposes a simple method based on the  $d$ -axis fundamental positive-sequence component of filter capacitor voltage feedforward (DFPS-CVFF) for three-phase PI controlled active damping LCL-type grid-connected converter. Under the proposed method, the start-up inrush current can be effectively suppressed without affecting the grid current quality and system stability under weak grid conditions. Furthermore, since the  $d$ -axis fundamental positive-sequence component of filter capacitor voltage is extracted from decoupled double synchronous reference frame phase-locked loop (DDSRF-PLL) [23], which uses the filter capacitor voltage for grid synchronization, the proposed method does not increase the extra sensors and software resources.

This paper is organized as follows. In Section 2, the mechanism of start-up inrush current is analyzed in detail. Then, the filter capacitor voltage feedforward, which is used to suppress start-up inrush current, is analyzed. In Section 3, DFPS-CVFF is proposed, and the influence of different feedforward methods on the system stability under weak grid conditions is analyzed by the impedance model of grid-connected converter. In Section 4, the experimental and simulation results demonstrate the validity of the proposed method. Finally, some conclusions are summarized in Section 5.

## 2. Generation and Suppression Mechanism Analysis of Start-Up Inrush Current

The three-phase LCL-type grid-connected converter topology and its control block in  $dq$  frame are shown in Figure 2. The LCL filter is composed of the converter side filter inductance  $L_1$ , filter capacitor  $C_f$ , and grid side filter inductance  $L_T$ , which is the leakage inductance of the isolation transformer. Grid current  $I_2$  is controlled by PI controller, and the capacitor current  $I_c$  feedback active damping is used to suppress the LCL filter resonance peak.  $I_1$  is the converter side current,  $U_{dc}$  is the DC-bus voltage,  $U_r$  is the converter output voltage, and  $U_{pcc}$  is the PCC voltage. For DPGSs, especially megawatt-level systems, it is relatively difficult to measure the PCC voltage to realize grid synchronization, due to the following reasons [24]: (1) the isolation transformer may be geographically far from the grid-connected converter; (2) in medium- or high-voltage applications, the PCC voltage is comparatively high, leading to a situation where the signal conditioning circuit can be quite complex and expensive; and (3) the grid side inductance of the LCL filter might be replaced by the leakage inductance of the isolation transformer to reduce the volume and cost, as in the system described in this paper. Therefore, as applied in [13,24,25], filter capacitor voltage  $U_c$  is used as the input voltage of DDSRF-PLL. Moreover, a weak grid can be denoted by the Thevenin equivalent circuit, in which an ideal grid voltage  $U_g$  is in series with the grid impedance  $L_g$ . The parameters of transformer high-voltage side  $U_g$ ,  $U_{pcc}$  and  $L_g$  are  $U'_g$ ,  $U'_{pcc}$  and  $L'_g$  after being converted to the transformer low-voltage side.

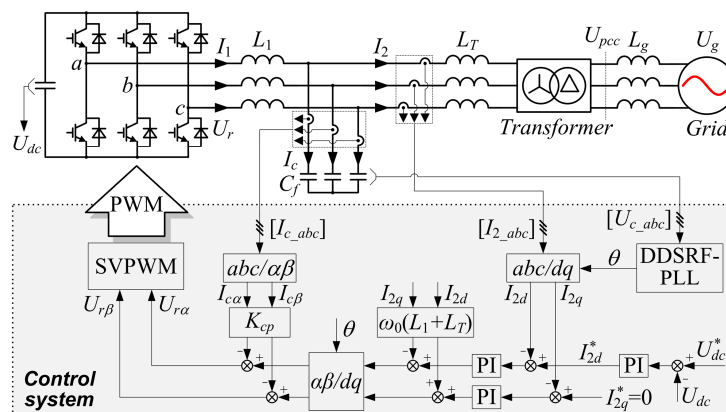


Figure 2. Topology and control block of three-phase LCL-type grid-connected converter.

### 2.1. Generation Mechanism Analysis of the Start-Up Inrush Current

Here,  $d$ -axis is used as an example. According to the main circuit of Figure 2, applying Kirchhoff's laws and Clarke transformation, (1) and (2) can be obtained:

$$-L_2\omega_0 I_{2q} + L_2 \frac{dI_{2d}}{dt} = U_{cd} - U'_{gd} \quad (1)$$

$$-L_1\omega_0 I_{1q} + L_1 \frac{dI_{1d}}{dt} = U_{rd} - U_{cd} \quad (2)$$

where  $L_2 = L_T + L'_g$  is the grid side equivalent inductance and  $\omega_0$  is the fundamental angular frequency. Subscripts " $d$ " and " $q$ " denote the  $d$ - and  $q$ -axis components, respectively.

Bellow the resonant frequency, the LCL filter behaves as an  $L$  filter. Therefore, by combining (1) and (2), the relationships among the grid voltage disturbances, the converter output control voltage and the current can be obtained, as shown in (3). It can be seen that the variety of grid current is determined by the  $U_{rd}$  and  $U'_{gd}$ .

$$L_2 \frac{dI_{2d}}{dt} + L_1 \frac{dI_{1d}}{dt} = U_{rd} - U'_{gd} \quad (3)$$

In Figure 2, the capacitor current feedback active damping in  $\alpha\beta$  frame can be equivalent to that in  $dq$  frame. Therefore, the control voltage  $U_{rd}$  of current loop output can be expressed as:

$$U_{rd} = K_p(I_{2d}^* - I_{2d}) + K_i \sum (I_{2d}^* - I_{2d})T_s - K_{cp}I_{cd} \quad (4)$$

where  $K_p$  and  $K_i$  are the proportional coefficient and integral coefficient, respectively, of the grid current PI controller.  $K_{cp}$  is the capacitor current feedback coefficient.  $T_s$  is sampling period.

Since the reference direction of grid current is from the converter to the grid, the grid current reference  $I_{2d}^*$  is negative when running in rectifier mode. According to (4), at the start time, since the  $I_{2d}$  and  $I_{cd}$  are very small,  $U_{rd}$  is negative. Then, according to (3),  $L_2 dI_{2d}/dt + L_1 dI_{1d}/dt$  will be large, and the current will increase quickly because of the superposition of  $U_{rd}$  and  $U'_{gd}$ . For the same trend of  $I_{2d}$  and  $I_{1d}$ , the grid current  $I_{2d}$  will increase rapidly, which leads to inrush current. Under weak grid conditions, the larger the grid inductance is (the larger  $L_2$  is), the smaller  $dI_{2d}/dt$  and inrush current will be. It can be concluded that, when grid voltage disturbance and converter output control voltage are in the same direction, the superposition of the two items will result in inrush current.

Then,  $U_{rd}$  has a process from negative to positive. When the  $U_{rd}$  is equal to  $U'_{gd}$ , the inrush current reaches the maximum value, which can be expressed as:

$$I_{peak} = \frac{-U'_{gd} + K_p I_{2d}^* + K_i \sum (I_{2d}^* - I_{2d})T_s - K_{cp}I_{cd}}{K_p} \quad (5)$$

In fact, according to (3) and (4), even if the current reference  $I_{2d}^* = 0$  when the converter starts; due to the disturbance of grid voltage and small values of  $I_{2d}$  and  $I_{cd}$ , the inrush current will also be aroused, but the inrush current peak is smaller than when current reference  $I_{2d}^*$  is negative. Therefore, start-up inrush current is not particularly dependent on the current reference.

Moreover, when the grid-connected converter starts in inverter mode, the current reference  $I_{2d}^*$  is positive. According to (4), due to the small values of  $I_{2d}$  and  $I_{cd}$  at start time, the  $U_{rd}$  is positive. Then, according to (3),  $L_2 dI_{2d}/dt + L_1 dI_{1d}/dt$  will be much smaller than that when converter starts in rectifier mode. Therefore, the inrush current is much smaller when the converter starts in inverter mode than that when converter starts in rectifier mode.

Since  $d$ -axis voltage is orientated on the grid voltage vector for control,  $q$ -axis grid voltage is zero. Therefore, the  $q$ -axis grid voltage does not cause disturbance to the grid current control, thus the start-up inrush current is mainly caused by  $d$ -axis voltage.

## 2.2. Suppression Mechanism Analysis of the Start-Up Inrush Current

For the above analysis, grid voltage disturbance is the primary cause of the start-up inrush current. Therefore, if this disturbance can be offset, the inrush current can be fundamentally suppressed. However, it is relatively difficult to measure the grid voltage or PCC voltage [24] as in the previous analysis, and therefore the filter capacitor voltage feedforward can be used to suppress the inrush current, since it is linear with the PCC voltage [13].

With the filter capacitor voltage feedforward compensation, the control voltage  $U'_{rd}$  of current loop output can be expressed as:

$$U'_{rd} = G_f U_{cd} + K_p (I_{2d}^* - I_{2d}) + K_i \sum (I_{2d}^* - I_{2d}) T_s - K_{cp} I_{cd} \quad (6)$$

where  $G_f$  is the feedforward function.

When the converter starts in rectifier mode, (7) can be obtained by combining (3), (4), (6) and (1).

$$L_1 \frac{dI_{1d}}{dt} = U_{rd} + G_f U_{cd} - U_{cd} \quad (7)$$

Comparison between (7) and (3) shows that, due to the same trends of  $I_{2d}$  and  $I_{1d}$ , with filter capacitor voltage feedforward, when  $G_f = K_f = 1$  ( $K_f$  is the feedforward proportional coefficient), the grid voltage disturbance is offset, and then  $L_1 dI_{1d}/dt$  will be smaller, the change rate of  $I_{2d}$  will be significantly decreased, and the inrush current will not be aroused. Under weak grid conditions, i.e., large  $L_2$ , according to (7), the filter capacitor voltage feedforward can also offset the grid voltage disturbance, and the inrush current can similarly be suppressed. When  $K_f$  is decreased from 1 to 0, due to the partial offset of grid voltage disturbance, the change rate of  $I_{2d}$  will be increased, and the inrush current suppression result will deteriorate. When  $K_f > 1$ , the grid voltage disturbance will be over-offset, which is not conducive to the dynamic performance and stability of the system. Therefore,  $G_f = K_f = 1$  is selected, and the maximum  $I_{2d}$  is:

$$I'_{peak} = \frac{-U'_{gd} + G_f U_{cd} + K_p I_{2d}^* + K_i \sum (I_{2d}^* - I_{2d}) T_s - K_{cp} I_{cd}}{K_p} \quad (8)$$

When the grid-connected converter starts in inverter mode or current reference  $I_{2d}^* = 0$ , (7) can be derived similarly. It also can be seen that the grid voltage disturbance can be effectively offset by capacitor voltage feedforward, so that the converter can also start without inrush current.

The filter capacitor voltage feedforward can offset the grid voltage disturbance and suppress the inrush current effectively. However, many grid current harmonics will be aroused and the system stability will deteriorate when the filter capacitor voltage feedforward is introduced under weak grid conditions. Therefore, in the next Section, the DFPS-CVFF will be proposed to suppress start-up inrush current without affecting the system stability under weak grid conditions.

## 3. The Proposed DFPS-CVFF Method

### 3.1. The Introduction of DFPS-CVFF

With filter capacitor voltage feedforward, the  $d$ -axis control block of grid current is shown in Figure 3.

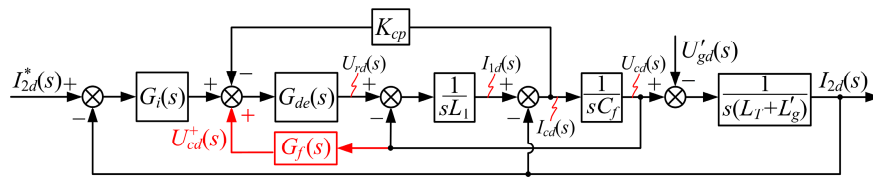


Figure 3. *d*-axis control block of grid current.

where filter capacitor voltage feedforward is shown as the red line of Figure 3,  $G_i(s) = K_p + K_i/s$  is PI controller of grid current.  $G_{de}(s)$  is the control delay, and it is expressed as in [10].

$$G_{de}(s) = e^{-1.5T_s s} \approx \frac{1 - 0.75sT_s}{1 + 0.75sT_s} \tag{9}$$

Figure 4 can be obtained by block transformation of Figure 3. It can be seen that, if  $G_f(s) = 1$ , the sampled filter capacitor voltage direct feedforward (SCVDFF) can be equivalent to the superposition of grid voltage feedforward and grid side equivalent inductance voltage feedforward, which contains the grid current and grid impedance information. Consequently, no matter whether it is in rectifier or inverter mode, it will introduce an additional positive feedback loop to the grid current, and the positive feedback loop will bring in the derivative function for grid impedance  $s(L_T + L'_g)$ , which will amplify the medium-high frequency harmonic and double-frequency disturbance in practical application, and seriously deteriorate the grid current quality and system stability under weak grid conditions. Moreover, the larger  $L'_g$  is, the more significant the effect of SCVDFF on grid current control will be.

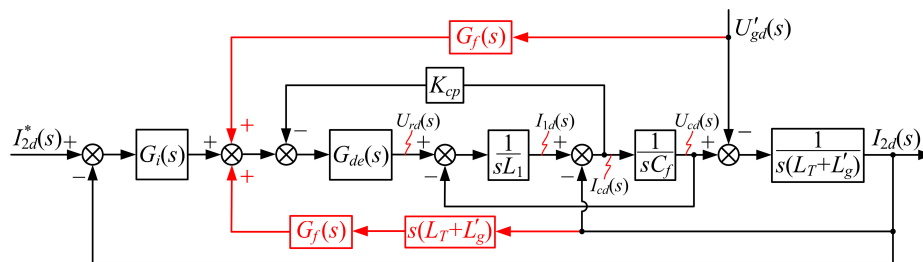


Figure 4. Equivalent control block of grid current.

If the transfer function of the additional positive feedback loop is changed, the grid current quality and system stability might be changed under weak grid conditions. Therefore, this paper proposes a method based on DFPS-CVFF to suppress the inrush current, while also improving the grid current quality and system stability under weak grid conditions. The *d*-axis fundamental positive-sequence component of capacitor voltage can be obtained by the decoupled network in DDSRF-PLL [23], as shown in Figure 5. This method does not increase the extra sensors and software resources, because the filter capacitor voltage is also used for grid synchronization. Note that, if the DDSRF-PLL is not used for grid synchronization, the *d*-axis fundamental positive-sequence component of capacitor voltage can also be obtained using the decoupling network algorithm of DDSRF-PLL.

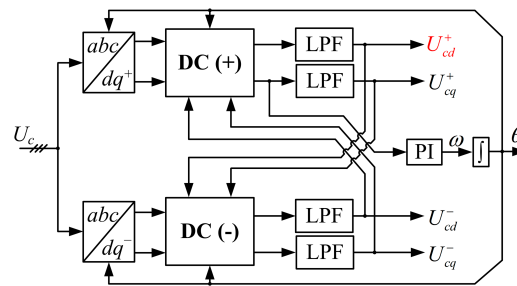


Figure 5. Control block of DDSRF-PLL.

As shown in Figure 5, the decoupling network can be approximated by a low-pass filter (LPF) cascading with a notch-filter tuned at  $2\omega_0$  [26]. Therefore, the equivalent fundamental positive-sequence component of capacitor voltage is:

$$\begin{bmatrix} U_{cd}^+(s) \\ U_{cq}^+(s) \end{bmatrix} = \frac{\omega_f}{s^2 + 2\omega_f s + \omega_0^2} \begin{pmatrix} s & -\omega_0 \\ \omega_0 & s \end{pmatrix} \begin{bmatrix} U_{cd}(s) \\ U_{cq}(s) \end{bmatrix} \quad (10)$$

where  $\omega_f$  is the cutoff angular frequency of LPF in DDSRF-PLL.

Due to the DDSRF-PLL,  $U_{cq} = 0$ . Then, the  $G_f(s)$  can be expressed as:

$$G_f(s) = \frac{\omega_f s}{s^2 + 2\omega_f s + \omega_0^2} \quad (11)$$

It can be seen that the decoupled network in DDSRF-PLL can completely eliminate the medium-high frequency harmonics and double-frequency disturbance of input voltage, and the positive- and negative-sequence voltages are decoupled. The additional positive feedback loop function of the grid current is also turned into  $G_f(s)s(L_T + L'_g)$ . As a result, the influence of the positive feedback loop on the grid current quality and system stability will be weakened significantly under weak grid conditions.

Note that, since the  $d$ -axis fundamental voltage component accounts for the largest of  $d$ -axis grid voltage, it is the main cause of start-up inrush current. And the  $d$ -axis fundamental positive-sequence component of filter capacitor voltage can be extracted by the decoupling network without phase error and with entire fundamental component [26]. Therefore, the inrush current suppression capability of DFPS-CVFF is the same as SCVDFF, which will be further verified by experiment.

When grid inductance  $L'_g = 0$ , filter capacitor voltage feedforward can be equivalent to the superposition of grid voltage feedforward and grid side inductance voltage feedforward. And grid voltage feedforward will contribute to reducing the negative effect of grid voltage harmonics and unbalanced grid on the grid current [5]. Therefore, this paper further proposes DFPS-CVFF expression as:

$$U_{cd}^+(s) = G_f(s)U_{cd}(s) = \left( K_{1f} \frac{\omega_f s}{s^2 + 2\omega_f s + \omega_0^2} + K_{2f} \right) U_{cd}(s) \quad (12)$$

where  $K_{1f}$  is the feedforward proportional coefficient of the  $d$ -axis fundamental positive-sequence component of filter capacitor voltage, and  $K_{2f}$  is the feedforward proportional coefficient of sampled filter capacitor voltage.

In order to effectively suppress the inrush current,  $K_{1f} + K_{2f} = K_f = 1$  should be selected. When  $K_{1f}$  is smaller and  $K_{2f}$  is larger, the grid voltage harmonics have a smaller effect on the grid current if grid inductance  $L'_g = 0$ . But under weak grid conditions, it will seriously affect the grid current quality and system stability. This paper mainly studies the start-up inrush current suppression and the influence of feedforward on the system stability, and grid voltage harmonics are beyond its scope. Therefore,

$K_{1f} = 1$  and  $K_{2f} = 0$  are selected. If the negative effect of grid voltage harmonics on the grid current needs to be considered under stiff grid conditions, the selection of  $K_{1f}$  and  $K_{2f}$  can be traded off.

Furthermore, the  $d$ -axis fundamental positive-sequence component of filter capacitor voltage is converted to the  $\alpha\beta$  frame to achieve feedforward. Thus, the  $\alpha\beta/dq$  transformation in the PLL and the  $dq/\alpha\beta$  transformation are canceled to avoid the PLL error effect under weak grid conditions. Then, DFPS-CVFF in the  $\alpha\beta$  frame can be expressed as:

$$\begin{cases} U_{ca}^+(s) = U_{cd}^+(s) \cos \theta \\ U_{cb}^+(s) = U_{cd}^+(s) \sin \theta \end{cases} \quad (13)$$

Finally, the overall control block of the grid-connected converter is shown in Figure 6, and the proposed DFPS-CVFF method is depicted as the red line of Figure 6. In the next subsection, the impedance model of the grid-connected converter will be used to analyze the influences of different feedforward methods on system stability under weak grid conditions.

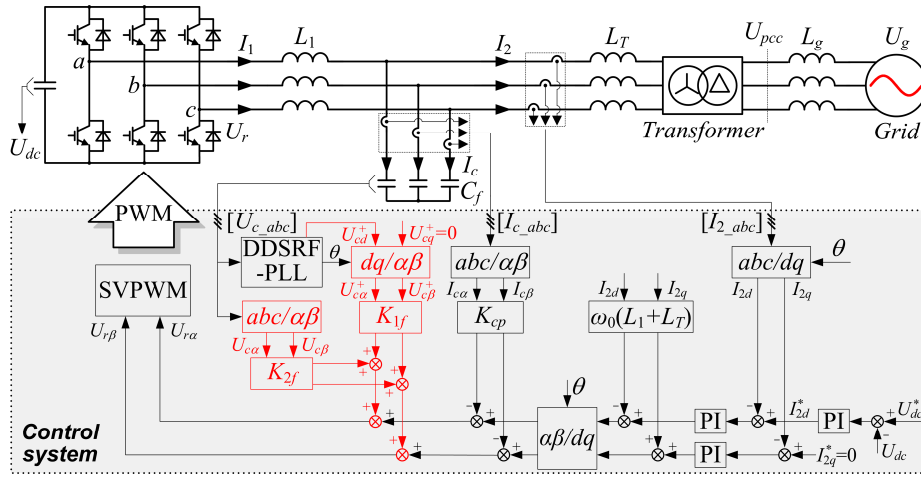


Figure 6. Control block of three-phase LCL-type grid-connected converter with proposed method.

### 3.2. Impedance-Based Stability Analysis under Weak Grid Conditions

In order to obtain the converter output impedance, the grid inductance is not included here. And Figure 7 can be obtained by block transformation of Figure 3.

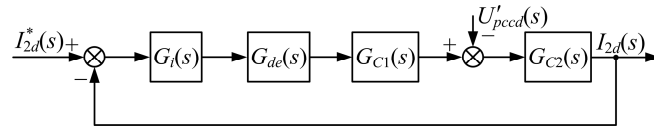


Figure 7. Grid current control block equivalent transformation.

where:

$$G_{C1}(s) = \frac{1}{s^2 L_1 C_f + s C_f K_{cp} G_{de}(s) + 1 - G_f(s) G_{de}(s)} \quad (14)$$

$$G_{C2}(s) = \frac{s^2 L_1 C_f + s C_f K_{cp} G_{de}(s) + 1 - G_f(s) G_{de}(s)}{s^3 L_1 L_T C_f + s^2 L_T C_f K_{cp} G_{de}(s) + s(L_T + L_1) - s L_T G_f(s) G_{de}(s)} \quad (15)$$

The loop gain  $T_A(s)$  of the system is:

$$T_A(s) = G_{C1}(s) G_{C2}(s) G_{de}(s) G_i(s) = \frac{G_i(s) G_{de}(s)}{s^3 L_1 L_T C_f + s^2 L_T C_f K_{cp} G_{de}(s) + s(L_T + L_1) - s L_T G_f(s) G_{de}(s)} \quad (16)$$

The grid current can be derived as:

$$I_{2d}(s) = \frac{T_A(s)}{1 + T_A(s)} I_{2d}^*(s) - \frac{G_{C2}(s)}{1 + T_A(s)} U'_{pccd}(s) \approx I_{od}(s) - \frac{U'_{pccd}(s)}{Z_{con}(s)} \quad (17)$$

where  $I_{od}(s)$  and  $Z_{con}(s)$  are the Norton equivalent current source and converter output impedance of  $d$ -axis respectively.  $Z_{con}(s)$  is shown as (18).

$$Z_{con}(s) = \frac{1+T_A(s)}{G_{C2}(s)} = \frac{s^3 L_1 L_T C_f + s^2 L_T C_f K_{cp} G_{de}(s) + s(L_T + L_1) - s L_T G_f(s) G_{de}(s) + G_i(s) G_{de}(s)}{s^2 L_1 C_f + s C_f K_{cp} G_{de}(s) + 1 - G_f(s) G_{de}(s)} \quad (18)$$

According to (17), the grid-connected converter can be equivalent to an ideal current source in parallel with converter output impedance. Similarly, the grid can be equivalent to an ideal voltage source in series with the grid impedance  $Z'_g(s)$ , as shown in Figure 8 [4,27].

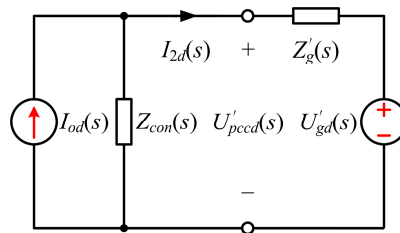


Figure 8. Equivalent circuit of grid-connected system.

According to Figure 8, the grid current can be expressed as:

$$I_{2d}(s) = \frac{Z_{con}(s)}{Z'_g(s) + Z_{con}(s)} I_{od}(s) - \frac{1}{Z'_g(s) + Z_{con}(s)} U'_{gd}(s) = \left( I_{od}(s) - \frac{U'_{gd}(s)}{Z_{con}(s)} \right) \frac{1}{1 + Z'_g(s)/Z_{con}(s)} \quad (19)$$

To guarantee robustness to grid impedance variation, the grid-connected converter should satisfy the following criteria [4,27,28]: (1) The current control is stable when  $Z'_g(s) = 0$ ; and (2) The impedance ratio  $Z'_g(s)/Z_{con}(s)$  satisfies the Nyquist criterion. That is, if the gains of  $Z_{con}(s)$  and  $Z'_g(s)$  intersect at the frequency  $f_{cross}$ , the phase margin at  $f_{cross}$  ( $PM_{cross}$ ) must be positive, i.e.,  $PM_{cross} > 0^\circ$ , and as large as possible.

The first criterion can be satisfied easily by designing the current controller properly. The second criterion is discussed here. Considering the worst situation, this paper supposes that grid impedance is a pure inductance, since the resistor in the grid impedance will increase the  $PM_{cross}$  and help to stabilize the system [4]. As a result, the phase of grid impedance is always  $90^\circ$ , and  $PM_{cross}$  can be expressed as:

$$PM_{cross} = 90^\circ + \arg(Z_{con}(2\pi f_{cross}j)) \quad (20)$$

A 10 kW three-phase LCL-type grid-connected converter is taken as an example. System parameters are listed in Table 1.

Table 1. System parameters of grid-connected converter.

Parameters	Values	Parameters	Values
Grid line-voltage $U_{gl}$	380 V	Converter side inductance $L_1$	3.2 mH
Grid frequency $f_0$	50 Hz	Filter capacitor $C_f$	15 $\mu$ F
Transformer ratio $N$	380/340	Transformer leakage inductance $L_T$	0.85 mH
Switching frequency $f_{sw}$	4.8 kHz	Current PI controller $K_p$	22
Sample frequency $f_s$	9.6 kHz	Current PI controller $K_i$	7000
DC-bus voltage $U_{dc}$	650 V	Capacitor current feedback coefficient $K_{cp}$	18

With different SCRs, Bode diagrams of grid-connected converter output impedance with no feedforward (NFF) ( $K_{1f} = K_{2f} = 0$ ), SCVDFF ( $K_{1f} = 0, K_{2f} = 1$ ) and DFPS-CVFF ( $K_{1f} = 1, K_{2f} = 0$ ) are shown in Figure 9a. When  $K_{1f} = 0, K_{2f}$  is changed, Bode diagrams of converter output impedance with SCVDFF are shown in Figure 9b. When  $K_{2f} = 0, K_{1f}$  is changed, Bode diagrams of converter output impedance with DFPS-CVFF are shown in Figure 9c. When both  $K_{2f}$  and  $K_{1f}$  are changed, and  $K_{1f} + K_{2f} = 1$ , Bode diagrams of converter output impedance are shown in Figure 9d.

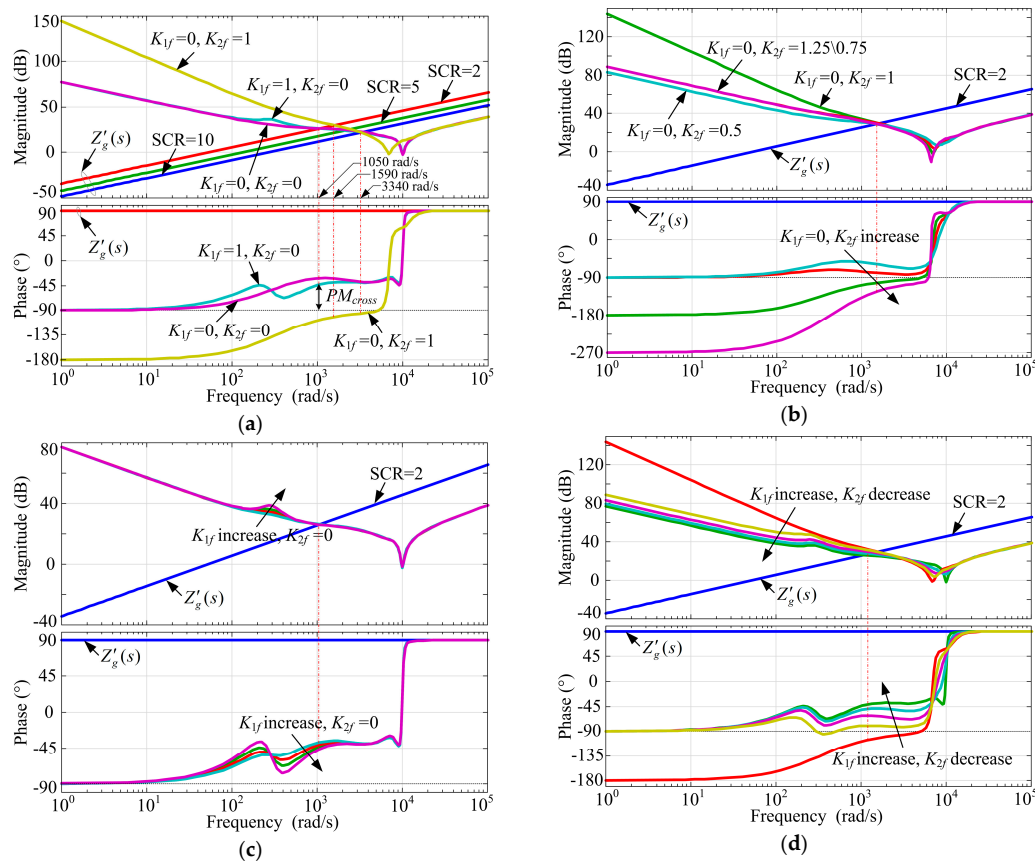


**Figure 9.** Bode diagrams of converter output impedance. (a)  $K_{1f} = K_{2f} = 0$ ;  $K_{1f} = 0, K_{2f} = 1$ ;  $K_{1f} = 1, K_{2f} = 0$ ; (b)  $K_{1f} = 0, K_{2f}$  changed; (c)  $K_{2f} = 0, K_{1f}$  changed; (d) Both  $K_{1f}$  and  $K_{2f}$  are changed, and  $K_{1f} + K_{2f} = 1$ .

As shown in Figure 9a, under the weak grid, the system has sufficient stability margin and  $PM_{cross}$  is always positive with NFF. With SCVDFF, the impedance magnitude is higher at low frequency ranges, which indicates that low frequency harmonic suppression ability is improved. However, the impedance phase decreases greatly and has negative behavior at low frequency, and  $PM_{cross}$  is negative, both of which seriously influence the system stability. The weaker the grid is, the smaller  $PM_{cross}$  is, and the worse system stability is. With DFPS-CVFF, the magnitude and phase of the converter output impedance are close to the NFF condition. The  $PM_{cross}$  is  $45^\circ$  when SCR = 2, and the system also has a sufficient stability margin under weak grid conditions. Therefore, DFPS-CVFF has better robustness against variations of grid impedance.

As shown in Figure 9b, with the SCVDFF, when  $K_{2f}$  is increased from 1 or reduced from 1, the low frequency amplitude of converter output impedance is decreased. With the increase of  $K_{2f}$ , the impedance phase is seriously decreased, and the stability of the system deteriorates. However, the decrease of  $K_{2f}$  is not conducive to the suppression of start-up inrush current, and the  $PM_{cross}$  is desired large enough. As shown in Figure 9c, with DFPS-CVFF, when  $K_{1f}$  is changed, there is little change in the magnitude and phase of the converter output impedance, and the  $PM_{cross}$  is always sufficient, both

of which have little influence on system stability. As shown in Figure 9d, with the increase of  $K_{1f}$  and decrease of  $K_{2f}$ , the converter output impedance magnitude at low frequency range is decreased, the phase is increased, and the stability margin of the system is increased.

In conclusion, the above analysis shows that (1) With SCVDFF, although the start-up inrush current of the grid-connected converter can be suppressed, the system stability will deteriorate seriously under weak grid conditions; and (2) With DFPS-CVFF proposed in this paper, it is not only possible to effectively suppress the start-up inrush current, but system stability is close to the NFF condition and will not be affected. The system has a stronger robustness under both stiff and weak grid conditions.

#### 4. Experimental and Simulation Results

To verify the above theoretical analysis, a prototype of a 10 kW three-phase LCL-type grid-connected converter is built, as shown in Figure 10. The topology is shown in Figure 2, and its parameters are listed in Table 1. The converter is implemented using an intelligent power module (IPM) (PM100RL1A120, Mitsubishi, Tokyo, Japan). The current and voltage are sensed by the halls (LA58-P, Lem, Beijing, China and CLSM-05MA, Sypris, Orlando, FL, USA). The control strategy is implemented in a DSP (TMS320F28335, Texas Instruments, Dallas, TX, USA). All the signals are sampled by a 12-bit A/D converter (AD7891, Analog Devices, Norwood, MA, USA). An isolation transformer is placed between the LCL-type grid-connected converter and the grid, and the leakage inductance  $L_T$  of the transformer acts as the grid side filter inductance of the LCL filter. An external inductance ( $L_g = 4.6$  mH and 23.1 mH, corresponding to SCR = 10 and 2, respectively) is used to emulate the weak grid, which is placed in series between the grid and the isolation transformer.

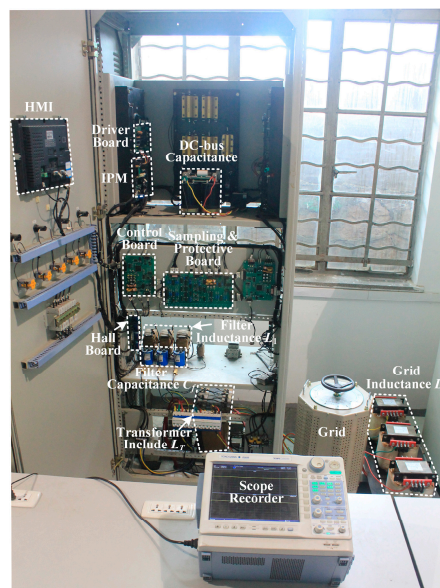


**Figure 10.** Prototype of the 10 kW three-phase LCL-type grid-connected converter.

Before converter start, phase locking is achieved, and the calculation of the  $d$ -axis fundamental positive-sequence component of capacitor voltage has already been completed.

##### 4.1. Under Normal Grid Voltage Conditions

When grid inductance  $L'_g = 0$ , experimental results of grid-connected converter starts in rectifier mode with NFF, SCVDFF and DFPS-CVFF are shown in Figure 11. The current reference is  $-10$  A. As shown in Figure 11a, with NFF, the current peak can reach 40 A, the overshoot is 300%. Obviously, such inrush current may trigger overcurrent protection, and even damage the switching device. However, with feedforward, as shown in Figure 11b,c, after a short adjustment, the grid current

converges smoothly to its reference, and the current peak has been effectively suppressed. Figure 11b,c also show that, with SCVDFE and DFPS-CVFE, the system has the same start-up inrush current suppression performance. Moreover, SCVDFE and DFPS-CVFE can offset the grid voltage disturbance, and the grid current has the better steady-state control performance compared with NFE.

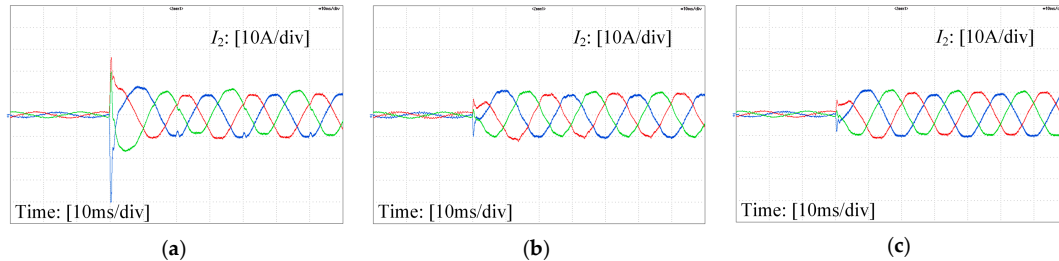


**Figure 11.** Grid-connected converter starting in rectifier mode. (a) NFE; (b) SCVDFE; (c) DFPS-CVFE.

When grid inductance  $L'_g = 0$ , experimental results of the grid-connected converter starting in inverter mode with NFE, SCVDFE and DFPS-CVFE are shown in Figure 12. The current reference is 10 A. The comparison of Figures 12a and 11a shows that the inrush current when the converter starts in inverter mode is much smaller than that when the converter starts in rectifier mode. With SCVDFE and DFPS-CVFE, the disturbance of grid voltage is restrained, and the grid-connected converter has a better start-up dynamic performance, which is consistent with the theoretical analysis.

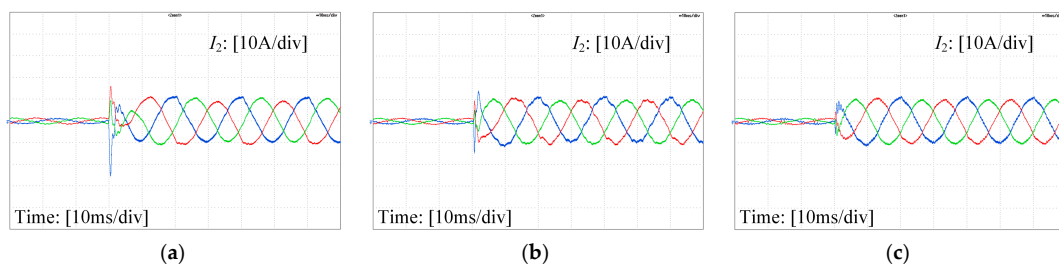


**Figure 12.** Grid-connected converter starting in inverter mode. (a) NFE; (b) SCVDFE; (c) DFPS-CVFE.

When grid inductance  $L'_g = 0$  and the current reference  $I_{2d}^* = 0$ , experimental results of the grid-connected converter starting with NFE, SCVDFE and DFPS-CVFE are shown in Figure 13. Figure 13a shows that even if the current reference  $I_{2d}^* = 0$  when the converter starts, the start-up inrush current is also aroused, and a little smaller than when the current reference is  $-10$  A, as shown in Figure 11a. This indicates that the start-up inrush current is not particularly dependent on the current reference, which is consistent with the theoretical analysis. The current peak can also be suppressed with SCVDFE and DFPS-CVFE, as shown in Figure 13b,c.

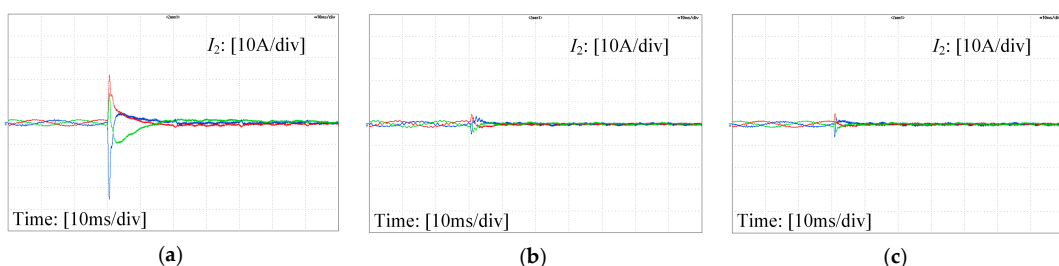


**Figure 13.** Grid-connected converter starting when current reference  $I_{2d}^* = 0$ . (a) NFE; (b) SCVDFE; (c) DFPS-CVFE.

When SCR = 10 and 2, experimental results of grid-connected converter starts in rectifier mode with NFF are shown in Figure 14, and the FFT analyses are shown in Figure 15. The comparison of Figure 14a,b and Figure 11a shows that, under weak grid conditions, with the increase of grid inductance, the start-up inrush current is smaller, which is consistent with the theoretical analysis.

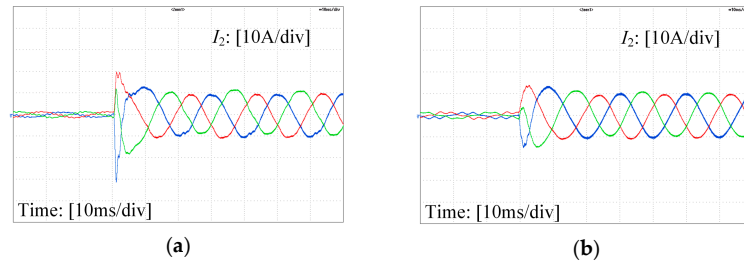


**Figure 14.** Grid-connected converter starting in rectifier mode with NFF. (a) SCR = 10; (b) SCR = 2.

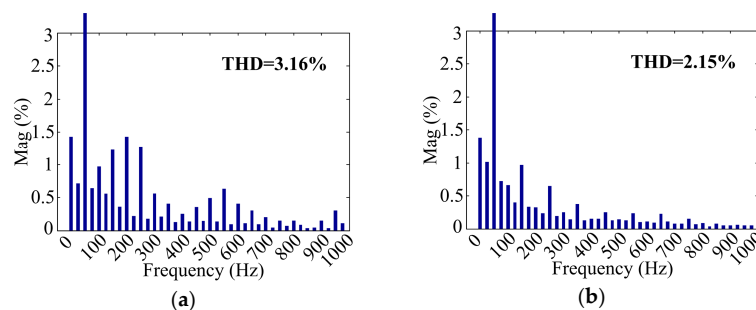


**Figure 15.** The FFT analysis of grid-connected converter starting in rectifier mode with NFF. (a) SCR = 10; (b) SCR = 2.

When SCR = 10 and 2, the experimental results for the grid-connected converter starting in rectifier mode with SCVDFF are shown in Figure 16, and the FFT analyses are shown in Figure 17. Under weak grid conditions, due to the additional positive feedback loop of grid current, the system does not have a big enough stability margin. Therefore, the grid current has many harmonics and serious distortion. The weaker the grid is, the more serious the grid current distortion will be. Moreover, as shown in Figure 9a, when SCR = 10 and 2, with SCVDFF, the converter output impedance intersects with the grid impedance around 550 Hz and 250 Hz, and the  $PM_{cross}$  is negative. This explains the distortion of grid current in Figure 16. FFT analysis of the grid current reveals large harmonics around the 550 Hz and 250 Hz respectively, as shown in Figure 17, which correlates to the impedance intersection frequency  $f_{cross}$ .

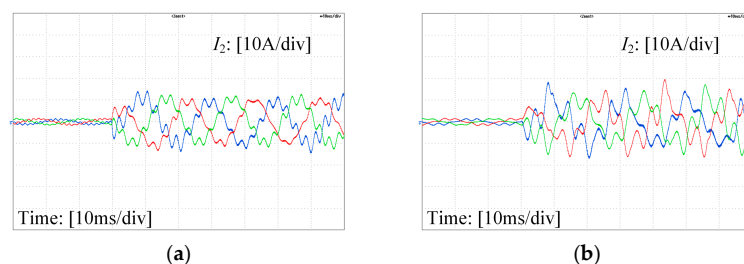


**Figure 16.** Grid-connected converter starting in rectifier mode with SCVDFF. (a) SCR = 10; (b) SCR = 2.

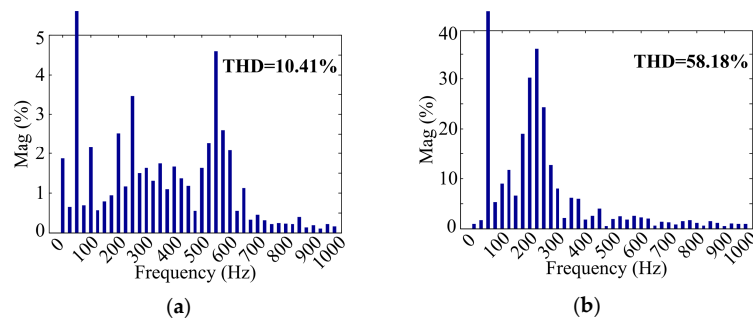


**Figure 17.** The FFT analysis of grid-connected converter starting in rectifier mode with SCVDFE. (a) SCR = 10; (b) SCR = 2.

When SCR = 10 and 2, the experimental results for the grid-connected converter starting in rectifier mode with DFPS-CVFF are shown in Figure 18, and the FFT analyses are shown in Figure 19. Under weak grid conditions, with DFPS-CVFF, the start-up inrush current can also be suppressed effectively. Since the system has a big enough stability margin, the grid current has better waveform quality compared with SCVDFE, as shown in Figure 16. The THD are smaller compared with NFF and SCVDFE, as shown in Figures 15 and 17. Moreover, the harmonics around the  $f_{cross}$  (550 Hz and 150 Hz) are significantly reduced compared with Figure 17, as shown in Figure 19, which illustrates the increase of  $PM_{cross}$  in Figure 9a.

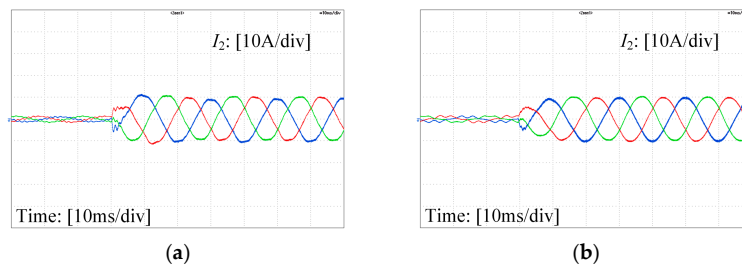


**Figure 18.** Grid-connected converter starting in rectifier mode with DFPS-CVFF. (a) SCR = 10; (b) SCR = 2.

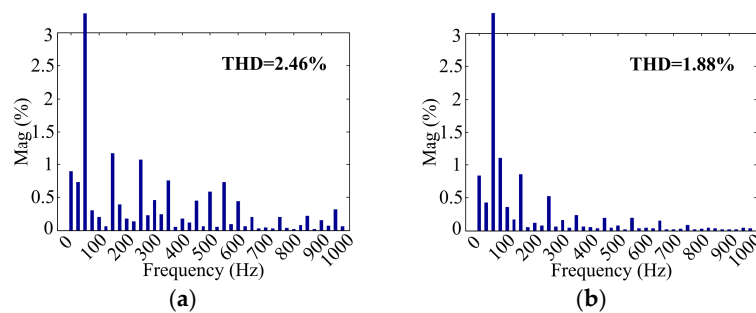


**Figure 19.** The FFT analysis of grid-connected converter starting in rectifier mode with DFPS-CVFF. (a) SCR = 10; (b) SCR = 2.

When grid inductance  $L'_g = 0$  and  $K_{1f} = 0$ ,  $K_{2f} = 0.75$  and  $0.25$ , respectively, the experimental results of the grid-connected converter starting in rectifier mode with SCVDFE are shown in Figure 20. When grid inductance  $L'_g = 0$  and  $K_{1f} = 0.75$ ,  $0.25$ ,  $K_{2f} = 0$ , respectively, the experimental results of the grid-connected converter starting in rectifier mode with DFPS-CVFF are shown in Figure 21. It can be seen that, under stiff grid conditions, the smaller the feedforward coefficient is, the worse the inrush

current suppression will be, which is consistent with the above theoretical analysis. Note that, except Figures 20 and 21, NFF is  $K_{1f} = K_{2f} = 0$ , SCVDFF is  $K_{1f} = 0, K_{2f} = 1$ , and DFPS-CVFF is  $K_{1f} = 1, K_{2f} = 0$ .

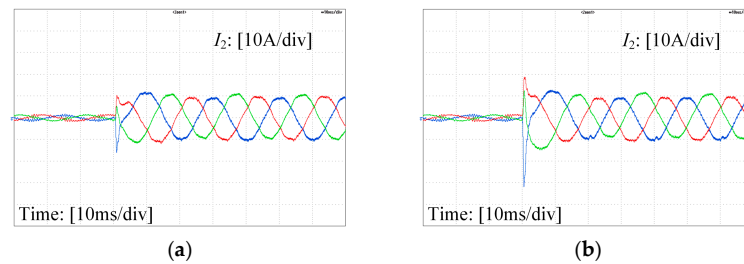


**Figure 20.** Grid-connected converter starting in rectifier mode with SCVDFF when grid inductance  $L'_g = 0$ . (a)  $K_{1f} = 0, K_{2f} = 0.75$ ; (b)  $K_{1f} = 0, K_{2f} = 0.25$ .

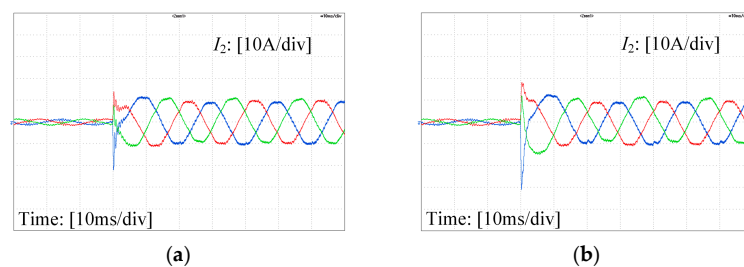


**Figure 21.** Grid-connected converter starting in rectifier mode with DFPS-CVFF when grid inductance  $L'_g = 0$ ; (a)  $K_{1f} = 0.75, K_{2f} = 0$ ; (b)  $K_{1f} = 0.25, K_{2f} = 0$ .

#### 4.2. Unbalanced and Distorted Grid Voltage Conditions

Since the weak grid often involves problems of unbalance and distortion, the effectiveness of the proposed control algorithm under the conditions of unbalanced and distorted grid voltage are also verified.

Under unbalanced grid voltage condition, the simulation results of the grid-connected converter starting in rectifier mode with DFPS-CVFF when  $L'_g = 0$ , SCR = 10, and SCR = 2, respectively, are shown in Figure 22. The grid voltage includes 20% voltage amplitude and zero phase shift of negative-sequence components. Figure 22 shows the filter capacitor line-voltage and grid current. The grid current is balanced, since the double synchronous reference frame PI controller [29] and DDSRF-PLL are used, and the start-up inrush current can also be suppressed effectively with the proposed method under unbalanced grid conditions.

Under unbalanced grid voltage conditions, the experimental results of the grid-connected converter starting in rectifier mode with DFPS-CVFF when  $L'_g = 0$ , SCR = 10, and SCR = 2, respectively, are shown in Figure 23. The phase-A and phase-B grid voltages are both dipped 20% using a grid fault generator [30]. Figure 23 shows the filter capacitor line-voltage and grid current. Note that the  $\Delta$ -Y type transformer will cause  $30^\circ$  phase shift of grid voltage and grid current. The experimental results also show that the start-up inrush current can also be suppressed effectively with the proposed method under unbalanced grid conditions.

Under distorted grid voltage conditions, the simulation results of the grid-connected converter starting in rectifier mode with DFPS-CVFF when  $L'_g = 0$ , SCR = 10, and SCR = 2, respectively, are shown in Figure 24. The grid voltage is distorted by 3% for fifth harmonics and 2% for seventh harmonics, with zero phase shifts. Figure 24 shows the filter capacitor line-voltage and grid current. Since the control strategy used in this paper cannot suppress the grid current harmonics caused by distorted grid voltage, there are some low-frequency harmonics in the grid current. However, this paper mainly focuses on start-up inrush current suppression, and the effect of the grid voltage harmonics is beyond

its scope. If further low frequency harmonic suppression is desired, other control schemes such as full-feedforward of grid voltages [11] or multiple proportional-resonant (PR) compensators [12] could be introduced. Moreover, Figure 24 also shows that the start-up inrush current can also be suppressed effectively with the proposed method under distorted grid conditions.

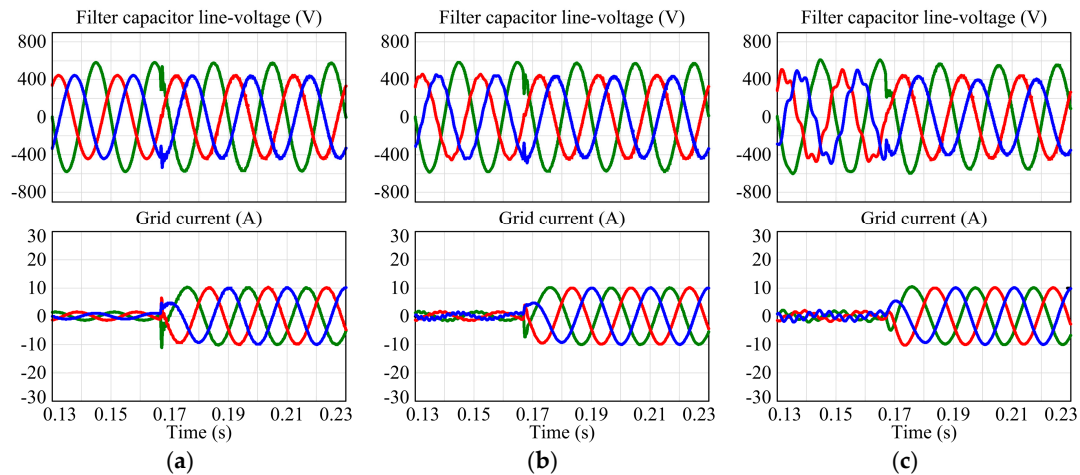


**Figure 22.** Simulation results of grid-connected converter starting in rectifier mode with DFPS-CVFF under unbalanced grid; (a)  $L'_g = 0$ ; (b) SCR = 10; (c) SCR = 2.

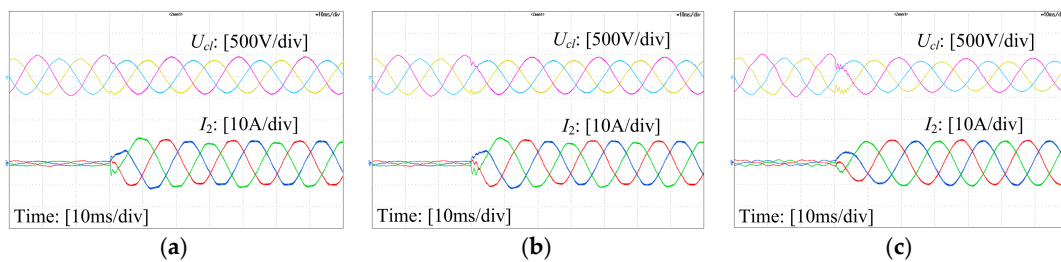


**Figure 23.** Experimental results of grid-connected converter starting in rectifier mode with DFPS-CVFF under unbalanced grid; (a)  $L'_g = 0$ ; (b) SCR = 10; (c) SCR = 2.

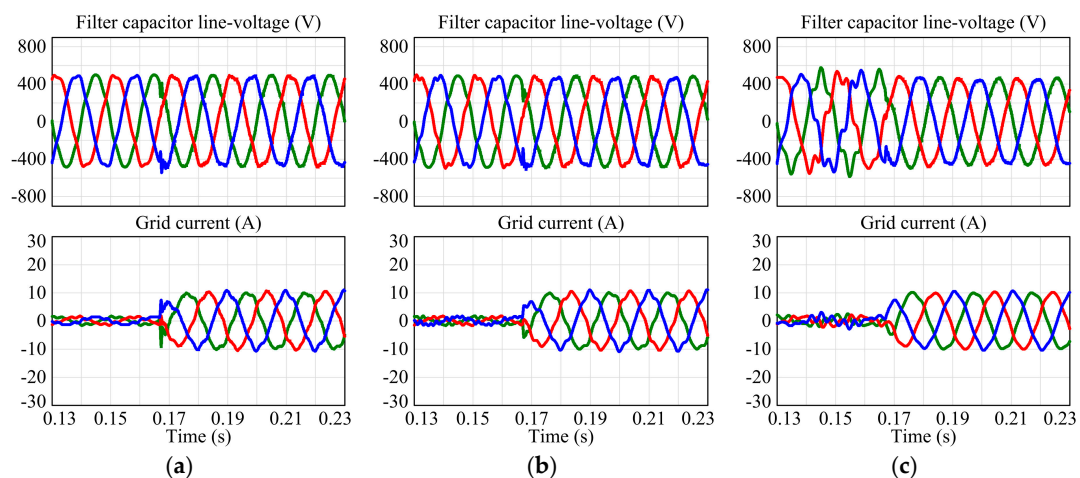


**Figure 24.** Simulation results of grid-connected converter starting in rectifier mode with DFPS-CVFF under distorted grid; (a)  $L'_g = 0$ ; (b) SCR = 10; (c) SCR = 2.

## 5. Conclusions

This paper proposes a simple method based on the DFPS-CVFF to suppress inrush current when a three-phase PI controlled active damping LCL-type grid-connected converter starts, while maintaining grid current quality and system stability under weak grid conditions. The main conclusions can be summarized as follows.

- The mechanism of inrush current when the grid-connected converter starts is deeply studied and it is concluded that, when the converter output voltage and the grid voltage disturbance are in the same direction, the superposition of the two items will result in serious inrush current. Under weak grid conditions, the larger the grid inductance is, the smaller the inrush current will be. Moreover, inrush current is the most serious when the converter starts in rectifier mode. The inrush current is much smaller when the converter starts in inverter mode than that when converter starts in rectifier mode. The start-up inrush current is not particularly dependent on the current reference. When the converter starts with zero current reference, the inrush current is also aroused, but the inrush current peak is smaller than that when the converter starts in the rectifier mode.
- The filter capacitor voltage feedforward can effectively suppress the start-up inrush current under both stiff and weak grid conditions, and the grid-connected converter has better start-up dynamic performance. With the decrease of the feedforward coefficient, the inrush current suppression result will deteriorate.
- With SCVDFF, the system stability margin seriously deteriorates under weak grid conditions. The weaker the grid is, the worse the system stability will be; and with the decrease of the feedforward coefficient, the system stability margin will increase under weak grid conditions. However, the DFPS-CVFF has little influence on system stability. The system has a stronger robustness under both stiff and weak grid conditions, and it has the same start-up inrush current suppression result as SCVDFF.
- The start-up inrush current can also be suppressed effectively with DFPS-CVFF under unbalanced and distorted grid voltage.

The proposed method can effectively suppress start-up inrush current, while maintaining grid current quality and system stability under weak grid conditions. Moreover, it does not increase the extra sensors and software resources.

**Acknowledgments:** This work was financially supported in part by the National Natural Science Foundations of China (NSFC) under Award 51477064, and in part by the National Key Research and Development Program of China under Award 2016YFB0900104.

**Author Contributions:** Shiyong Zhou proposed the main idea and performed the theoretical analysis; Li Tong contributed to the main idea; Xudong Zou and Yong Kang contributed the experiment materials; Shiyong Zhou and Donghai Zhu performed the experiments; Shiyong Zhou wrote the paper; Xudong Zou and Donghai Zhu gave some suggestions to the paper writing.

**Conflicts of Interest:** The authors declare no conflict of interest.

## References

1. Blaabjerg, F.; Teodorescu, R.; Liserre, M.; Timbus, A.V. Overview of control and grid synchronization for distributed power generation systems. *IEEE Trans. Ind. Electron.* **2006**, *53*, 1398–1409. [[CrossRef](#)]
2. Zhang, W.; Remon, D.; Cantarellas, A.M.; Rodriguez, P. A unified current loop tuning approach for grid-connected photovoltaic inverters. *Energies* **2016**, *9*, 723. [[CrossRef](#)]
3. Liserre, M.; Teodorescu, R.; Blaabjerg, F. Stability of photovoltaic and wind turbine grid-connected inverters for a large set of grid impedance values. *IEEE Trans. Power Electron.* **2006**, *21*, 263–272. [[CrossRef](#)]
4. Yang, D.; Ruan, X.; Wu, H. Impedance shaping of the grid-connected inverter with LCL filter to improve its adaptability to the weak grid condition. *IEEE Trans. Ind. Electron.* **2014**, *29*, 5795–5805. [[CrossRef](#)]

5. Xu, J.; Xie, S.; Tang, T. Improved control strategy with grid-voltage feedforward for LCL-filter-based inverter connected to weak grid. *IET Power Electron.* **2014**, *7*, 2660–2671. [[CrossRef](#)]
6. Zhou, S.; Zou, X.; Zhu, D.; Kang, Y.; Tong, L.; Gao, X. LCL type grid-connected converter no startup inrush current control method based on capacitor branch voltage feedforward. In Proceedings of the 41th Annual Conference on IEEE Industrial Electronics Society (IECON), Yokohama, Japan, 9–12 November 2015; pp. 1471–1476.
7. Wang, X.; Blaabjerg, F.; Loh, P.C. Grid-current-feedback active damping for LCL resonance in grid-connected voltage-source converters. *IEEE Trans. Power Electron.* **2016**, *31*, 213–223. [[CrossRef](#)]
8. Yao, W.; Yang, Y.; Zhang, X.; Blaabjerg, F.; Loh, P.C. Design and analysis of robust active damping for LCL filters using digital notch filters. *IEEE Trans. Power Electron.* **2017**, *32*, 2360–2375. [[CrossRef](#)]
9. Zhang, N.; Tang, H.; Yao, C. A systematic method for designing a PR controller and active damping of the LCL filter for single-phase grid-connected PV inverters. *Energies* **2014**, *7*, 3934–3954. [[CrossRef](#)]
10. Wu, X.; Li, X.; Yuan, X.; Geng, Y. Grid harmonics suppression scheme for LCL-type grid-connected inverters based on output admittance revision. *IEEE Trans. Sustain. Energy* **2015**, *6*, 411–421. [[CrossRef](#)]
11. Li, W.; Ruan, X.; Pan, D.; Wang, X. Full-feedforward schemes of grid voltages for a three-phase LCL-type grid-connected inverter. *IEEE Trans. Ind. Electron.* **2013**, *60*, 2237–2250. [[CrossRef](#)]
12. Liserre, M.; Teodorescu, R.; Blaabjerg, F. Multiple harmonics control for three-phase grid converter systems with the use of PI-RES current controller in a rotating frame. *IEEE Trans. Power Electron.* **2006**, *21*, 836–841. [[CrossRef](#)]
13. Li, X.; Fang, J.; Tang, Y.; Wu, X.; Geng, Y. Capacitor voltage feedforward with full delay compensation to improve weak grids adaptability of LCL-filtered grid-connected converters for distributed generation systems. *IEEE Trans. Power Electron.* **2017**, in press. [[CrossRef](#)]
14. Chen, C.; Xiong, J.; Wan, Z.; Lei, J.; Zhang, K. A time delay compensation method based on area equivalence for active damping of an LCL-type converter. *IEEE Trans. Power Electron.* **2017**, *32*, 762–772. [[CrossRef](#)]
15. Qu, B.; Hong, X.; Lv, Z. A study of startup inrush current of three-phase voltage source PWM rectifier with PI controller. In Proceedings of the IEEE International in Power Electronics and Motion Control Conference (IPEMC-ECCE Asia), Wuhan, China, 17–20 May 2009; pp. 980–983.
16. Khajehoddin, S.A.; Karimi-Ghartemani, M.; Jain, P.K.; Bakhshai, A. A control design approach for three-phase grid-connected renewable energy resources. *IEEE Trans. Sustain. Energy* **2011**, *2*, 423–432. [[CrossRef](#)]
17. Gu, B.G.; Choi, J.H.; Jung, I.S. Start-up current control method for three-phase PWM rectifiers with a low initial DC-link voltage. *J. Power Electron.* **2012**, *12*, 587–594. [[CrossRef](#)]
18. Yao, X.; Wang, X. Research on new method of improvement of the dynamic ability for PWM rectifier. In Proceedings of the IEEE Conference and Expo in Transportation Electrification Asia-Pacific (ITEC Asia-Pacific), Beijing, China, 31 August–3 September 2014; pp. 1–5.
19. He, J.; Jun, Y.; Gong, B.; Lei, J.; Liu, Y.; Long, F. Analysis of start-up inrush current and its mitigation control strategy for grid connected voltage source inverter. In Proceedings of the IEEE Conference and Expo in Transportation Electrification Asia-Pacific (ITEC Asia-Pacific), Beijing, China, 31 August–3 September 2014; pp. 1–4.
20. Radwan, A.A.A.; Mohamed, Y.A.R.I. Improved vector control strategy for current-source converters connected to very weak grids. *IEEE Trans. Power Syst.* **2016**, *31*, 3238–3248. [[CrossRef](#)]
21. Chen, X.; Zhang, Y.; Wang, S.; Chen, J.; Gong, C. Impedance-phased dynamic control method for grid-connected inverters in a weak grid. *IEEE Trans. Power Electron.* **2017**, *1*, 274–283. [[CrossRef](#)]
22. Tang, Y.; Huang, L.; Zhao, G. Resonant feed forward control for LCL-type grid-tied inverters in weak grid condition. In Proceedings of the IEEE Energy Conversion Congress and Exposition (ECCE), Milwaukee, WI, USA, 18–22 September 2016; pp. 1–6.
23. Rodriguez, P.; Pou, J.; Bergas, J.; Candela, J.I.; Burgos, R.P.; Boroyevich, D. Decoupled double synchronous reference frame PLL for power converters control. *IEEE Trans. Power Electron.* **2007**, *22*, 584–592. [[CrossRef](#)]
24. Lu, M.; Xin, Z.; Wang, X.; Beres, R.N.; Blaabjerg, F. Extended stable boundary of LCL-filtered grid-connected inverter based on an improved grid-voltage feedforward control. In Proceedings of the IEEE Energy Conversion Congress and Exposition (ECCE), Milwaukee, WI, USA, 18–22 September 2016; pp. 1–7.
25. Huang, Y.; Yuan, X.; Hu, J.; Zhou, P.; Wang, D. DC-bus voltage control stability affected by AC-bus voltage control in VSCs connected to weak AC grids. *IEEE J. Emerg. Sel. Top. Power Electron.* **2016**, *4*, 445–458. [[CrossRef](#)]

26. Golestan, S.; Monfared, M.; Freijedo, F.D. Design-oriented study of advanced synchronous reference frame phase-locked loops. *IEEE Trans. Power Electron.* **2013**, *28*, 765–778. [[CrossRef](#)]
27. Yu, Y.; Li, H.; Li, Z.; Zhao, Z. Modeling and analysis of resonance in LCL-type grid-connected inverters under different control schemes. *Energies* **2017**, *10*, 104. [[CrossRef](#)]
28. Sun, J. Impedance-based stability criterion for grid-connected inverters. *IEEE Trans. Power Electron.* **2011**, *26*, 3075–3078. [[CrossRef](#)]
29. Song, H.; Nam, K. Dual current control scheme for PWM converter under unbalanced input voltage conditions. *IEEE Trans. Ind. Electron.* **1999**, *46*, 953–959. [[CrossRef](#)]
30. Zhu, D.; Zou, X.; Deng, L.; Huang, Q.; Zhou, S.; Kang, Y. Inductance-emulating control for DFIG-based wind turbine to ride-through grid faults. *IEEE Trans. Power Electron.* **2017**, in press. [[CrossRef](#)]



© 2017 by the authors. Licensee MDPI, Basel, Switzerland. This article is an open access article distributed under the terms and conditions of the Creative Commons Attribution (CC BY) license (<http://creativecommons.org/licenses/by/4.0/>).